BIOLOGICAL CRYSTALLOGRAPHY

ISSN 1399-0047

Full-length structure of the major autolysin LytA

Qiong Li,[a]‡ Wang Cheng,[a]‡ Cécile Morlot,[b,c,d] Xiao-Hui Bai,[a] Yong-Liang Jiang,[a] Wenjia Wang,[e] David I. Roper,[f] Thierry Vernet,[b,c,d] Yu-Hui Dong,[e] Yuxing Chen[a]* and Cong-Zhao Zhou[a]*

[a]Hefei National Laboratory for Physical Sciences at the Microscale and School of Life Sciences, University of Science and Technology of China, Hefei, Anhui 230027, People's Republic of China, [b]Universite Grenoble Alpes, Institut de Biologie Structurale (IBS), F-38027 Grenoble, France, [c]CEA, DSV, IBS, F-38027 Grenoble, France, [d]CNRS, IBS, F-38027 Grenoble, France, [e]Beijing Synchrotron Radiation Facility, Institute of High Energy Physics, Chinese Academy of Sciences, Beijing 100049, People's Republic of China, and [f]School of Life Sciences, University of Warwick, Gibbet Hill Road, Coventry CV4 7AL, England. *Correspondence e-mail: cyxing@ustc.edu.cn, zcz@ustc.edu.cn

Received 2 December 2014
Accepted 15 April 2015

Edited by Q. Hao, University of Hong Kong

‡ These authors contributed equally to this work.

Keywords: *Streptococcus pneumoniae*; crystal structure; peptidoglycan; autolysin; dimerization; choline-binding sites.

PDB reference: LytA, 4x36

Supporting information: this article has supporting information at journals.iucr.org/d

LytA is responsible for the autolysis of many *Streptococcus* species, including pathogens such as *S. pneumoniae*, *S. pseudopneumoniae* and *S. mitis*. However, how this major autolysin achieves full activity remains unknown. Here, the full-length structure of the *S. pneumoniae* LytA dimer is reported at 2.1 Å resolution. Each subunit has an N-terminal amidase domain and a C-terminal choline-binding domain consisting of six choline-binding repeats, which form five canonical and one single-layered choline-binding sites. Site-directed mutageneses combined with enzymatic activity assays indicate that dimerization and binding to choline are two independent requirements for the autolytic activity of LytA *in vivo*. Altogether, it is suggested that dimerization and full occupancy of all choline-binding sites through binding to choline-containing TA chains enable LytA to adopt a fully active conformation which allows the amidase domain to cleave two lactyl-amide bonds located about 103 Å apart on the peptidoglycan.

1. Introduction

Peptidoglycan (PG), the main component of the cell wall, is essential for bacterial survival, and its synthesis and degradation are closely related to cell growth and division. Tailoring and recycling of the PG requires the cleavage of different covalent bonds of the PG sacculi by specific hydrolases (Vollmer *et al.*, 2008). The cell wall of various pathogens, including *Streptococcus pneumoniae*, contains choline groups on the cell-wall teichoic acids (TA) and the membrane-associated lipoteichoic acids (Tomasz, 1967). Some of the cell-wall hydrolases, which belong to the family of choline-binding proteins (CBPs), bind noncovalently to these choline groups through their choline-binding domain (CBD; Gosink *et al.*, 2000). The CBD usually contains multiple choline-binding repeats (CBRs) that share the consensus sequence GWXK-X_{4-5}WYYφX_{3-5}GXMX_{2-3} (where X is any residue and φ is a hydrophobic residue; Hermoso *et al.*, 2005; Molina *et al.*, 2009).

In *S. pneumoniae*, the major autolysin LytA is a CBP that is responsible for the autolytic process occurring during the stationary phase (Mosser & Tomasz, 1970). Autolysis promotes the release of a variety of virulence factors, including the intracellular pneumolysin and soluble fragments of PG and TA (Cockeran *et al.*, 2002; Tuomanen *et al.*, 1985; Seo *et al.*, 2008). LytA specifically recognizes the nascent PG which becomes accessible after the release of the cell-wall

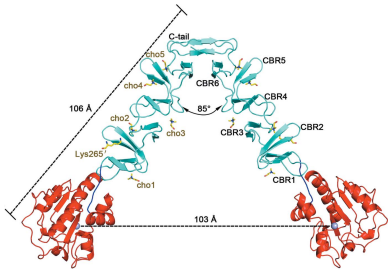

synthesis machinery at the end of the logarithmic phase, leading to the subsequent autolytic process in the stationary phase (Mellroth *et al.*, 2012). LytA consists of an N-terminal amidase domain followed by a CBD containing six putative CBRs and a C-terminal tail (Usobiaga *et al.*, 1996; Varea *et al.*, 2000). Upon binding to choline, LytA dimerizes, a process leading to activation of the hydrolase to its full activity (Höltje & Tomasz, 1976; Tomasz & Westphal, 1971). Dimerization is mediated by the last CBR and the C-terminal tail (Usobiaga *et al.*, 1996; Varea *et al.*, 2000) and is required for high levels of hydrolytic activity towards purified cell walls (Sánchez-Puelles *et al.*, 1987; Varea *et al.*, 2000), suggesting that the physiologically active LytA is a dimer. Intriguingly, LytA shows comparable *in vitro* hydrolytic activity towards TA-free pneumococcal cell wall and PG purified from Gram-negative bacteria such as *Escherichia coli* and *Pseudomonas putida* (Díaz *et al.*, 1996; Severin *et al.*, 1997). The role of the choline-binding properties in the activation mechanism of LytA therefore remains mysterious.

In past decades, investigations of the activation mechanism of LytA have led to three major structural reports. In 2001, Tornero and coworkers solved the crystal structure of the CBD (residues Gly192–Lys318), which forms a boomerang-like dimer with an internal angle of 85° (PDB entry 1hcx; Fernández-Tornero *et al.*, 2001). The CBD exhibits a left-handed superhelical structure which contains six β-hairpins corresponding to the C-terminal tail and five CBRs. In this structure, the last CBR and the C-terminal tail of two LytA subunits cross each other at an almost perpendicular dihedral angle, resulting in a stable dimeric interface. In each subunit, the authors identified four choline-binding sites (CBSs) at the interfaces of five consecutive CBRs. Subsequently, they reported another dimeric form of the CBD covering residues Thr224–Lys318, which exhibits an internal angle of 110° (PDB entry 1h8g; Fernández-Tornero *et al.*, 2002). Based on these two conformations of the LytA dimer, they proposed a step-by-step walking model on the PG (Fernández-Tornero *et al.*, 2002). Recently, Mellroth and coworkers reported the crystal structure of the LytA amidase domain ($LytA^{AMI}$; PDB entry 4ivv) and revealed a Y-shaped substrate-binding groove which was proposed to hydrolyze large substrates that are only available in cell-wall regions containing nascent PG (Mellroth *et al.*, 2014). Despite the important structural insights provided by these studies of truncated LytA domains, elucidation of the molecular mechanism of LytA activation at the cell wall still requires structural information on the entire protein. Here, we report the crystal structure of full-length LytA bound to choline at 2.1 Å resolution. This structure unifies the previous observations since it shows that the N-terminal α/β mixed amidase domains from two LytA subunits are connected through the boomerang-like association of the superhelical CBDs. This structure also establishes the presence of six CBRs and six CBSs in each LytA subunit for the first time. We functionally and structurally investigated the involvement of these six CBSs and the C-terminus in LytA activity, which revealed that both dimerization and full choline occupancy of all CBSs are required for full activity of LytA *in vivo*.

2. Materials and methods

2.1. Cloning, expression and purification of LytA

The coding region for LytA/Sp_1937 was cloned into a pET-22b-derived expression vector. The construct was over-expressed in *E. coli* strain BL21 (DE3) cells grown in LB medium containing 50 µg ml^{-1} ampicillin and 0.1 m*M* $ZnCl_2$. The transformed cells were grown at 37°C to an $A_{600\ nm}$ of 0.8 and then induced with 0.2 m*M* isopropyl β-D-1-thiogalacto-pyranoside (IPTG) for a further 4 h before harvesting. The cells were collected by centrifugation at 8000*g* for 10 min and resuspended in 40 ml lysis buffer (20 m*M* Tris–HCl pH 7.5, 50 m*M* NaCl). After 20 min of sonication and centrifugation at 16 000*g* for 30 min, the supernatant containing the soluble target protein was collected and loaded onto a DEAE Sefinose column pre-equilibrated with binding buffer (20 m*M* Tris–HCl pH 7.5, 50 m*M* NaCl). The target protein was eluted with binding buffer containing 250 m*M* choline chloride and further loaded onto a Superdex 200 column pre-equilibrated with 20 m*M* Tris–HCl pH 7.5, 100 m*M* NaCl, 10 m*M* choline chloride. Fractions containing the target protein were collected and concentrated to 15 mg ml^{-1} for crystallization. For enzymatic activity assays, the protein was purified using a buffer consisting of 50 m*M* Na_2HPO_4/NaH_2PO_4 pH 7.0, 10 m*M* choline chloride.

Selenomethionine (SeMet)-labelled LytA protein was expressed in *E. coli* strain B834 (DE3). Transformed cells were grown at 37°C in SeMet medium (M9 medium supplemented with 25 µg ml^{-1} SeMet and the other amino acids at 50 µg ml^{-1}) containing 50 µg ml^{-1} ampicillin and 0.1 m*M* $ZnCl_2$ to an $A_{600\ nm}$ of 0.8 and were then induced with 0.2 m*M* IPTG for a further 4 h. SeMet-substituted LytA was purified using the protocol that was used for native LytA.

2.2. Crystallization, data collection and processing

Crystals of SeMet-substituted LytA were grown at 289 K using the hanging-drop vapour-diffusion method by mixing 1 µl protein solution with an equal volume of reservoir solution (1.3 *M* ammonium tartrate dibasic, 0.1 *M* bis-tris propane pH 7.0). Crystals were transferred to a cryoprotectant solution (reservoir solution supplemented with 25% glycerol) and flash-cooled with liquid nitrogen. The SeMet-derivative data for a single crystal were collected at 100 K in a liquid-nitrogen gas stream on beamline 17U at the Shanghai Synchrotron Radiation Facility (SSRF) using an ADSC Quantum 315r CCD (MAR Research). All diffraction data were integrated and scaled with *HKL*-2000 (Otwinowski & Minor, 1997).

2.3. Structure determination and refinement

The crystal structure of LytA was determined using the single-wavelength anomalous dispersion phasing method (Brodersen *et al.*, 2000). Using the selenium anomalous signal, the selenium sites were located with *phenix.solve* implemented in *PHENIX* (Adams *et al.*, 2010). The initial model was built automatically using *AutoBuild* in *PHENIX*. The SeMet-substituted model was further refined by the maximum-

Table 1
Crystal parameters, data collection and structure refinement of SeMet-substituted LytA.

Values in parentheses are for the highest resolution bin.

Data collection	
Space group	$P4_32_12$
Wavelength (Å)	0.97923
Unit-cell parameters (Å)	$a = b = 101.28$, $c = 119.58$
Resolution range (Å)	50.00–2.10 (2.18–2.10)
Unique reflections	36872 (3622)
Completeness (%)	99.8 (100.0)
$\langle I/\sigma(I)\rangle$	17.0 (4.9)
$R_{\rm merge}$† (%)	8.9 (46.9)
$CC_{1/2}$	0.999 (0.980)
Wilson B factor (Å^2)	38.2
Matthews coefficient (Å^3 Da^{-1})	4.20
Average multiplicity	9.3 (9.4)
Anomalous completeness (%)	99.9 (100.0)
Anomalous multiplicity	12.7 (12.5)
Phasing statistics	
Model correlation coefficient	0.88
Figure of merit	0.51
Structure refinement	
Resolution range (Å)	46.63–2.10
No. of reflections	36872
$R_{\rm work}$‡/$R_{\rm free}$§ (%)	18.28/19.90
No. of atoms	
Protein	2596
Water	241
Ligands	12
B factors (Å^2)	
Protein	42.1
Water	49.0
Ligands	53.9
R.m.s.d.¶	
Bond lengths (Å)	0.008
Bond angles (°)	1.084
Ramachandran plot†† (% of residues)	
Most favoured	98.74
Additional allowed	1.26
PDB entry	4x36

† $R_{\rm merge} = \sum_{hkl}\sum_i |I_i(hkl) - \langle I(hkl)\rangle| / \sum_{hkl}\sum_i I_i(hkl)$, where $I_i(hkl)$ is the intensity of an observation and $\langle I(hkl)\rangle$ is the mean value for its unique reflection; summations are over all reflections. ‡ R factor = $\sum_{hkl} ||F_{\rm obs}| - |F_{\rm calc}|| / \sum_{hkl} |F_{\rm obs}|$, where $F_{\rm obs}$ and $F_{\rm calc}$ are the observed and calculated structure-factor amplitudes, respectively. § $R_{\rm free}$ was calculated with 5% of the data, which were excluded from the refinement. ¶ Root-mean-square deviation from ideal values. †† Categories were defined by *MolProbity*.

likelihood method implemented in *REFMAC*5 (Murshudov *et al.*, 2011) as part of the *CCP*4 (Winn *et al.*, 2011) program suite and rebuilt interactively with *Coot* (Emsley & Cowtan, 2004). The final model was evaluated with *MolProbity* (Chen *et al.*, 2010) and *PROCHECK* (Laskowski *et al.*, 1993). The crystallographic parameters are listed in Table 1. All figures showing the structure were prepared with *PyMOL* (DeLano, 2002).

2.4. Preparation of other versions of LytA

Both the individual LytA amidase domain (Met1–Asn170) used in the enzymatic activity assays and full-length LytA prepared for the measurement of secondary-structure composition were cloned into a pET-28-derived expression vector with an N-terminal 6×His tag. The constructs were transformed into *E. coli* strain BL21 (DE3) cells grown in LB medium containing 30 µg ml^{-1} kanamycin and 0.1 m*M* $ZnCl_2$. The transformed cells were grown at 37°C and induced with 0.2 m*M* IPTG at an $A_{600\,\rm nm}$ of 0.8. After a further 4 h of incubation at 37°C, the cells were harvested, resuspended and sonicated. After centrifugation, the target protein was purified by a combination of affinity chromatography using Ni–NTA resin and size-exclusion chromatography using a Superdex 200 column. The buffer used for purification of the LytA amidase domain consisted of 50 m*M* Na_2HPO_4/NaH_2PO_4 pH 7.0, 10 m*M* choline chloride, whereas the full-length LytA was purified using a buffer consisting of 50 m*M* Na_2HPO_4/NaH_2PO_4 pH 7.0.

Truncated LytA (Met1–Lys304) without the C-terminal tail was constructed and purified in the same manner as the full-length LytA without a 6×His tag. The other LytA mutants in this work were obtained using the Mut Express Fast Mutagenesis Kit with the plasmid encoding wild-type LytA as the template. The mutants were expressed and purified in the same manner as the wild-type protein without a 6×His tag.

2.5. Molecular docking

The putative substrate NAM-Pep5 was docked into the LytA amidase domain with *AutoDock* 4.2 (Morris *et al.*, 2009), which uses a unique algorithm that implements a machine-learning approach in its scoring function. The docking gave a large number of possible conformations and orientations for the substrate in a given pocket. The protein LytA and the substrate were converted from the PDB format to the PDBQT format. All single bonds within the substrate were set to allow rotation. The docking area was assigned as a grid box with dimensions of 20 × 25 × 40 points, in which the substrate could move freely. The results were sorted by binding affinity and visually analyzed in *PyMOL*.

2.6. Hydrolytic activity assays

PG with choline-containing TA from *S. pneumoniae* TIGR4 was prepared following a previously described protocol (Morlot *et al.*, 2010). Purified TA-containing cell walls were dyed with Remazol Brilliant Blue R (RBB; Sigma) according to a previous report (Zhou *et al.*, 1988). Briefly, purified PG was incubated with 20 m*M* RBB in 0.25 *M* NaOH overnight at 37°C and then neutralized with 0.25 *M* HCl. The dye-labelled PG was centrifuged at 21 000*g* for 20 min at 20°C. The RBB-labelled PG was then washed six times with ddH_2O to remove free RBB and was then lyophilized.

Each reaction was performed at 37°C in a 150 µl system containing 0.5 mg ml^{-1} RBB-labelled PG and 2 µ*M* protein in 50 m*M* Na_2HPO_4/NaH_2PO_4 pH 7.0. The reaction was terminated at different time points by heating to 95°C for 5 min. Afterwards, the supernatants containing the soluble RBB-labelled products were collected by centrifugation at 21 000*g* for 20 min at 20°C and the absorbance at 595 nm was determined using a Beckman DU800 spectrophotometer. All experiments were performed three times.

2.7. Turbidometric assays

The lytic activity of LytA towards live *S. pneumoniae* cells was detected by measuring the decrease in turbidity after

treatment with recombinant LytA protein. The *lytA* mutant strain was a gift from Professor Jing-Ren Zhang at Tsinghua University. It has a chromosomal insertion at the *lytA* gene locus of *S. pneumoniae* TIGR4. The *lytA* mutant strain was grown in THY medium until the early stationary phase and was then collected by centrifugation. The cells were resuspended in THY medium to an optical density at 600 nm of 0.8. Purified wild-type LytA was added to the cells to a final concentration of 10 μg ml^{-1} and the decrease in turbidity (absorption at 600 nm) was monitored at 37°C at 20 s intervals for 20 min using a Beckman DU800 spectrophotometer. The lytic activities of the LytA CBS mutants, the LytA amidase domain and LytA$^{1–304}$ were tested in the same manner as the wild type. All experiments were performed three times.

2.8. Circular-dichroism (CD) spectrometry

LytA and its mutants were purified in a buffer consisting of 50 m*M* Na_2HPO_4/NaH_2PO_4 pH 7.0, 10 m*M* choline using the protocol used to purify the proteins for crystallization. The choline-containing LytA was diluted to 0.08 mg ml^{-1} in the same buffer and its secondary-structure composition was analyzed using a Jasco J-810 spectropolarimeter. Spectra were recorded from 190 to 280 nm with an interval of 0.5 nm at room temperature. The final spectra represent the average data from three consecutive scans. Choline-free LytA was purified as described above and its secondary structure was analyzed in the same manner.

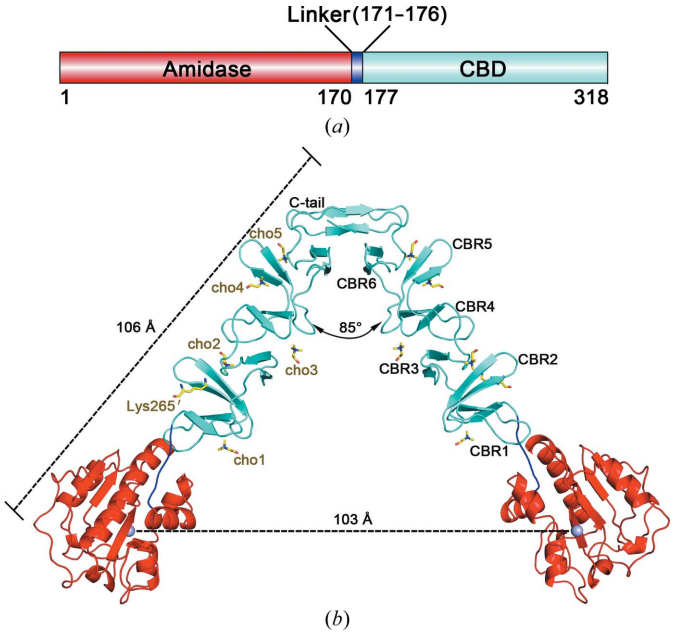

Figure 1
Overall structure of LytA. (*a*) Domain organization of LytA. (*b*) Structure of the dimeric LytA. The N-terminal amidase domain, linker and C-terminal CBD are shown in red, blue and cyan, respectively. The six CBRs and the C-terminal tail are labelled sequentially. Five choline molecules and Lys265′ from the neighbouring molecule are shown as yellow sticks. The arm length and the distance between two zinc ions are shown in Å.

3. Results

3.1. Overall structure of full-length LytA

Each asymmetric unit of the crystal contains one molecule of LytA (Supplementary Fig. S1), which is organized as an N-terminal globular amidase domain (Met1–Asn170) connected to a C-terminal cylindrical CBD (Gly177–Lys318) *via* a six-residue linker (Gly171–Thr176) (Fig. 1*a*). This structure enabled us to identify six CBRs, termed CBR1 to CBR6 from the N-terminus to the C-terminus (Fig. 1*b*). A symmetry operation yielded a LytA homodimer with a total buried interface area of 991 Å^2, which is mediated by the C-terminal tail and CBR6 (Supplementary Fig. S2), similar to the previously reported structures of the CBD of LytA (LytA-CBD; Fernández-Tornero *et al.*, 2001, 2002). The two LytA subunits, which are related by a twofold symmetric axis, form a boomerang-like structure with an internal angle of 85° and two arms of 106 Å in length (Fig. 1*b*). The two amidase domains at the N-termini mimic the two blades of the boomerang, with the two catalytic zinc ions positioned 103 Å apart. Superposition of our LytA dimer on the two previously reported CBDs (PDB entries 1hcx and 1h8g) yielded a root-mean-square deviation (r.m.s.d.) of 1.34 Å over 244 C$^\alpha$ atoms and 4.40 Å over 179 C$^\alpha$ atoms, respectively (Supplementary Fig. S3). Notably, the full-length structure adopts the same internal angle as the first reported CBD structure that comprises five CBRs per subunit (PDB entry 1hcx; Fernández-Tornero *et al.*, 2001), but differs from the second structure, which displays an internal angle of 110° (PDB entry 1h8g; Fernández-Tornero *et al.*, 2002). The observed variation in the internal angle reflects the flexibility between the two arms of boomerang-like dimer of LytA, a feature likely to be linked to the previously proposed step-by-step walking process of LytA at the cell wall (Fernández-Tornero *et al.*, 2002).

3.2. The amidase domain

The amidase domain of LytA (LytA-amidase) adopts a mixed α/β fold comprising a central five-stranded β-sheet sandwiched by five α-helices and two η-helices on both sides (Fig. 2*a*). The back side of the β-sheet is shielded from the solvent by helices α2 and α5, whereas the front side and helices α1, α3, η1 and η2, in addition to several loops, form a largely solvent-exposed valley. A search against the *DALI* database (http://ekhidna.biocenter.helsinki.fi/dali_server/; Holm & Rosenström, 2010) with the structure of LytA-amidase indicates that it resembles other amidase_2 members and is particularly similar to the structure of the catalytic domain of the *Staphylococcus aureus* autolysin AmiA (AmiA-cat; PDB entry 4knk; Büttner *et al.*, 2014), with a *Z*-score of 21.5 and an r.m.s.d. of 1.8 Å over 164 C$^\alpha$ atoms (Fig. 2*b*).

At the centre of the solvent-exposed valley, a zinc ion is coordinated by a water molecule (Wat1) and the side chains of His26, His133 and Asp149 (Fig. 2*a*), and combines with the catalytic residues Glu87 and His147, which have been proposed to facilitate a water-mediated nucleophilic attack on the lactyl-amide bond and to stabilize the reaction intermediate, respectively (Zoll *et al.*, 2010). Interestingly, in the

structure of LytA^{AMI} reported by Mellroth and coworkers the zinc ion coordination involves three water molecules (Mellroth *et al.*, 2014), whereas in our structure only one water molecule (Wat1) is adequately positioned to participate in the zinc coordination (Supplementary Fig. S4). In LytA^{AMI} (PDB entry 4ivv), one of the additional water molecules is indirectly stabilized by His147, whereas the other forms a direct hydrogen bond to the O atom in the main chain of Asp73 (Mellroth *et al.*, 2014). Similar to our LytA-amidase structure, only one water molecule is involved in coordination of the zinc ion present in the active site of unliganded *S. aureus* AmiA-cat (PDB entry 4knk), whereas two water molecules in the active site of liganded AmiA-cat (PDB entry 4knl) participate in coordination of the zinc ion (Supplementary Fig. S4; Büttner *et al.*, 2014). These differences in the water-coordination pattern of the zinc ion might represent intermediate activation states and/or intermediate catalytic states.

The crystal structure shows that LytA-amidase contains an extended Y-shaped groove, with three clefts meeting at the zinc-containing active site (Fig. 2*c*). A recent report proposed that this Y-shaped groove accommodates the glycan chain and the peptide stem of nascent PG (Mellroth *et al.*, 2014). No mimicking synthetic substrate is commercially available. We therefore tried to obtain the structure of LytA in complex with the simpler *N*-acetylmuramyl-L-alanyl-D-isoglutamyl-L-lysyl-L-alanyl-L-alanine (NAM-Pep5) substrate, but did not succeed. Alternatively, we performed docking experiments using *AutoDock* 4.2 (Morris *et al.*, 2009) to model the accommodation of substrate in the groove of LytA-amidase. We chose to dock NAM-Pep5 in order to compare the result of our molecular modelling with the experimental data reported for the binding of a muramyltetrapeptide (MurNac-L-Ala-D-iGln-L-Lys-NHAc-D-Ala-NH$_2$) in the catalytic groove of AmiA-cat (Büttner *et al.*, 2014). In our docking model, the NAM moiety is embedded in one of the negatively charged clefts, whereas the pentapeptide moiety lies in the relatively hydrophobic cleft (Fig. 2*c*). In detail, the NAM moiety is hydrogen-bonded by Thr28, Lys45 and His147, with the hexose ring stacking against Phe52 (Fig. 2*d*). With regard to the pentapeptide stem, the main-chain N and carboxyl O atoms of the D-iGln form hydrogen bonds to Asp73, Gly75 and Asn79. In contrast, the side chain of D-iGln points outwards and does not interact with any residue along the groove. This orientation allows the groove to accommodate different peptides with a variable second residue, consistent with the previous report that pneumococcal LytA can hydrolyze *E. coli* PG, which harbours a D-Glu at the counterpart position to D-iGln (Weidel & Pelzer, 1964). The L-Lys

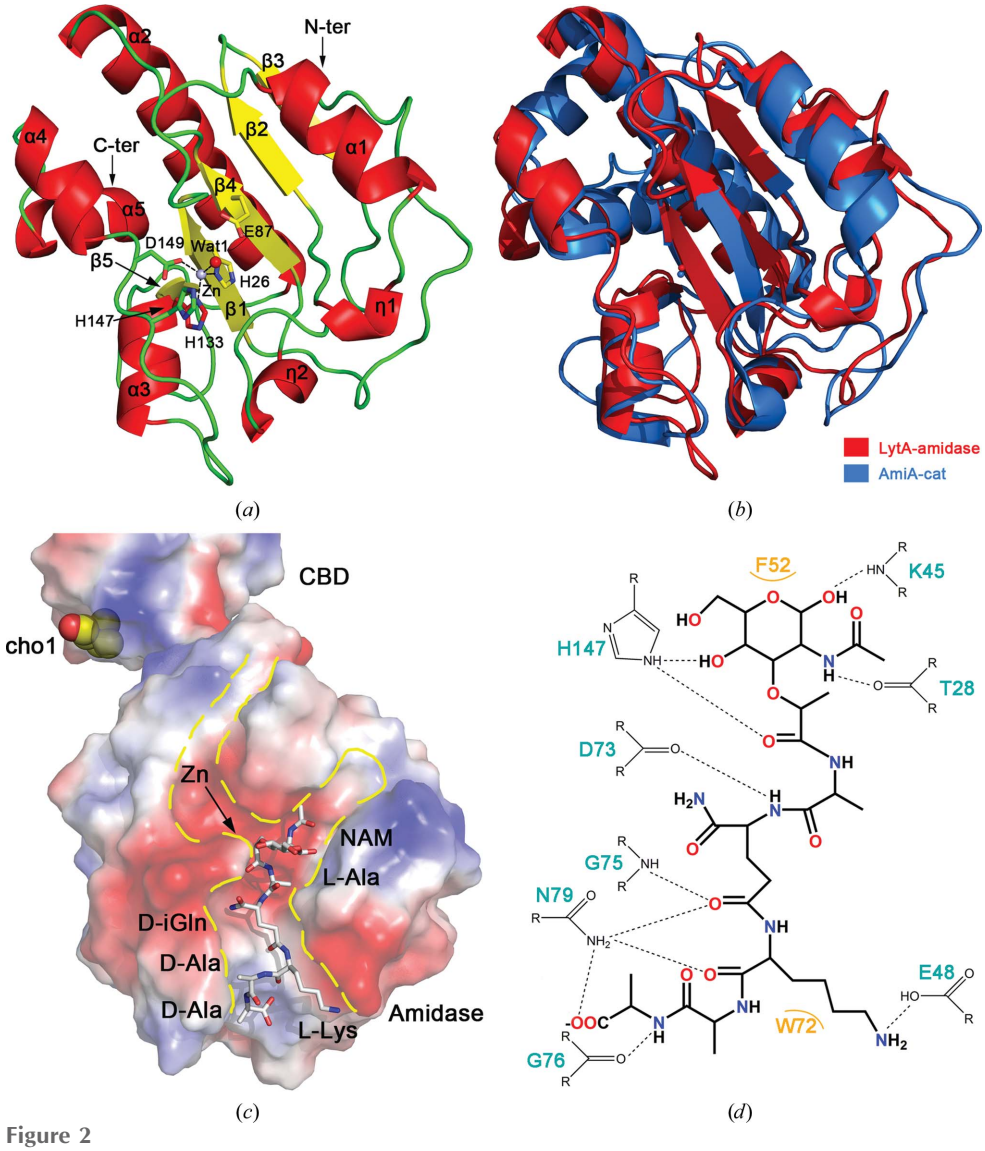

Figure 2
The amidase domain of LytA. (*a*) Cartoon representation of the pneumococcal LytA amidase domain. Helices, β-strands and loops are coloured red, yellow and green, respectively. The zinc ion and its coordinating water molecule are displayed as light blue and red spheres, respectively. The active-site residues are shown as sticks. (*b*) Structural superposition of *S. pneumoniae* LytA-amidase (in red) on *S. aureus* AmiA-cat (blue; PDB entry 4knk). (*c*) Electrostatic potential diagram of LytA with docked NAM-Pep5. NAM-Pep5 is shown as grey sticks. The outlines of the Y-shaped groove are shown with dashed lines. (*d*) A scheme showing the interactions between NAM-Pep5 and LytA. Hydrophobic interactions are depicted as yellow arcs, whereas hydrogen bonds are shown as black dashed lines.

at the third position appears to be well accommodated, with its main-chain carboxyl O atom hydrogen-bonded to Asn79 and its side chain stabilized by Trp72 and Glu48 *via* π-stacking and a salt bridge, respectively. The last D-Ala residue forms two hydrogen bonds to Gly76 and Asn79 (Fig. 2*d*).

As shown in Supplementary Fig. S5, the docked NAM-Pep5 superimposes well on the muramyltetrapeptide substrate in the structure of liganded AmiA-cat (Büttner *et al.*, 2014). In further support of the docking model, three molecules of glycerol, which was used for cryoprotection, are present in the putative substrate-binding groove of LytA. Two glycerol molecules occupy the spaces of the docked L-Lys and D-Ala moieties of NAM-Pep5, whereas the third glycerol is found in the cleft accommodating the docked NAM moiety (Supplementary Fig. S6).

3.3. The choline-binding domain

A close analysis of the structure of LytA-CBD enabled us to divide it into six CBRs in addition to a C-terminal β-hairpin tail. Subsequent sequence alignment of the six CBRs clearly showed a consensus sequence GW*X*KX_{4-5}WYYφX_{3-5}G*X*M-X_{2-3} (Fig. 3*a*), in agreement with previous reports (Hermoso *et al.*, 2005; Molina *et al.*, 2009). Each pair of consecutive CBRs forms a canonical CBS, which contains two hydrophobic layers. Taking the CBS between CBR3 and CBR4 as an example, the inner layer is composed of three aromatic residues (Trp/Phe, Trp and Tyr) and a hydrophobic residue (Met/Leu), whereas the outer layer consists of three hydrophobic residues in addition to a Lys residue stacked against the inner aromatic Trp (Fig. 3*b*). Each canonical CBS binds to a choline molecule, except for the CBS between CBR1 and CBR2, which is occupied by the side chain of Lys265′ from a neighbouring LytA molecule owing to crystal packing (Fig. 1*b* and Supplementary Fig. S7). However, at the junction between CBR1 and the N-terminal amidase domain, we found an extra CBS, which has only a single layer composed of three aromatic residues, Trp186 and Tyr194 from CBR1 in addition to Tyr214 from CBR2 (Fig. 3*c*), and which should result in a relatively lower affinity towards choline. The dimer is capable of binding to a total of 12 choline molecules, mediating the anchoring of LytA to the cell wall. The LytA-CBD in our structure displays 93% sequence identity and almost identical CBSs to the CBD of LytA from the pneumococcal prophage (Mellroth *et al.*, 2014). Superposition of the CBD in the two structures yields an r.m.s.d. of 1.0 Å over 146 C^{α} atoms. Moreover, the prophage CBD dimer displays an internal angle of 85°, identical to the LytA-CBD in our structure. We suggest that LytA becomes rather rigid upon full occupancy of choline molecules in the two CBD subunits.

3.4. The interdomain linker

Despite the crystal structures of the individual amidase domain and the CBD of LytA having been previously reported (Fernández-Tornero *et al.*, 2001, 2002; Mellroth *et al.*, 2014), the interdomain cross-talk remained unknown owing to the lack of a high-resolution structure of full-length LytA. Here, our structure revealed that a total interface area of 156.3 Å^2 is buried between the two domains. In addition, the two domains are bridged by a six-residue hydrophobic linker (Fig. 4*a*). At the interdomain interface, the main-chain O atom of Ser190 from the CBD forms two hydrogen bonds to the side-chain N atoms of Arg103 in the amidase domain (Fig. 4*b*). On one hand, the N-terminal residues Gly171, Leu172 and Ile174 of the linker form a hydrogen bond and hydrophobic interactions with Asp167, Met99 and Tyr102 from LytA-amidase, respectively. On the other hand, the C-terminal Thr176 of the linker interacts with the CBD *via* a hydrogen bond to the side chain of Gln179, which forms a main-chain hydrogen bond to Trp186, a key residue in the single-layered CBS. In contrast, the central residues (Thr173 and Ile174) of

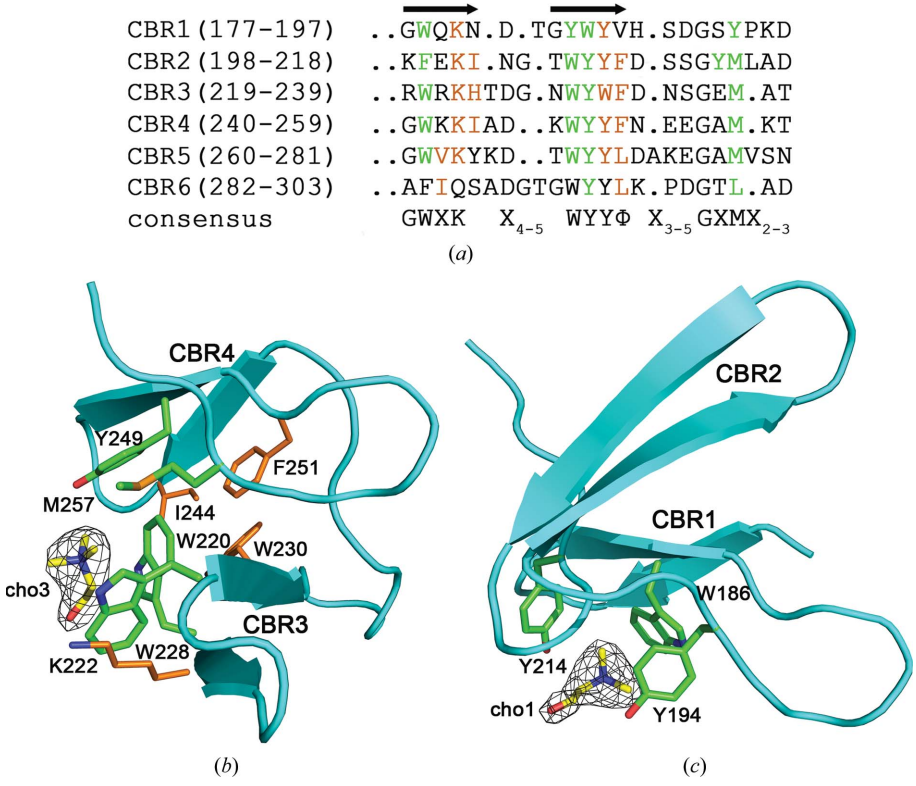

Figure 3
Sequence and structural analyses of the choline-binding sites. (*a*) Sequence alignment of the six CBRs. The residues constituting the inner and outer layers of the CBS are coloured green and orange, respectively. (*b*) The canonical CBS binding to cho3. (*c*) The single-layered CBS binding to cho1. Residues involved in the inner and outer layers are shown as green and orange sticks, respectively. The choline molecules are displayed as yellow sticks.

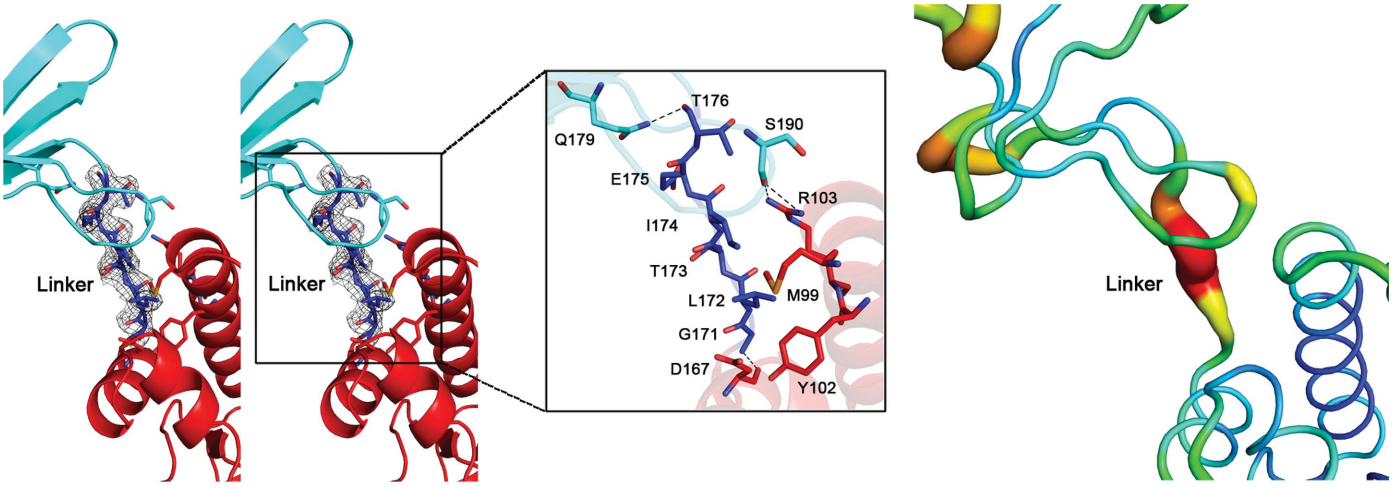

Figure 4
The linker between the amidase domain and the CBD. (*a*) The OMIT electron-density map ($2F_o - F_c$) of the linker is contoured at the 1.0σ level. The amidase domain, linker and CBD are shown in red, blue and cyan, respectively. (*b*) A close-up view of the interdomain interface. Interacting residues are shown as sticks. Hydrogen bonds are indicated as dashed lines. (*c*) A *B*-factor tube diagram of the linker. Regions with higher *B* factors are shown with a line of larger diameter and are coloured red.

the linker have relatively higher *B* factors (Fig. 4*c*), indicating that the junction between the two domains is somewhat dynamic.

3.5. Both dimerization and full occupancy of all choline-binding sites are indispensable for *in vivo* activity of LytA

Although the individual amidase domain of LytA is able to bind nascent PG (Mellroth *et al.*, 2012), LytA-amidase had no detectable autolytic activity in the turbidometric assays (Fig. 5*a*), indicating that the CBD is required for *in vivo* autolytic activity (Garcia-Bustos & Tomasz, 1987). The CBD of each LytA molecule contains five canonical CBSs and a single-layered CBS. To further determine the contribution of these CBSs to the activity of LytA, we used turbidometric assays to compare the autolytic activity of wild-type LytA and mutants carrying double mutations in all six CBSs. The results showed that all double mutations at either type of CBS led to complete loss of activity (Fig. 5*a*).

In parallel, these proteins were applied to *in vitro* hydrolytic activity assays towards purified TA-containing pneumococcal cell wall. LytA-amidase exhibits almost no hydrolytic activity (Fig. 5*b*). The double mutation Y194A/Y214A in the single-layered CBS resulted in only a reduced initial hydrolytic velocity, whereas double mutations in the five canonical CBSs led to a significant reduction in both the initial hydrolytic velocity and the final yield of soluble products (Fig. 5*b*). However, all double mutants exhibit a comparable decrease in autolytic activity (Fig. 5*a*), demonstrating that the initial hydrolytic velocity is critical for the *in vivo* activity of LytA. Together, the full occupancy of choline molecules in all CBSs is crucial for LytA catalysis.

Notably, circular-dichroism spectra showed that all of the mutants exhibit a secondary-structure composition similar to the wild-type protein, indicating that their loss of activity is owing to impaired choline-binding properties rather than folding defects (Supplementary Fig. S8*a*). Analysis of the LytA mutants by size-exclusion chromatography indicated that they form stable homodimers. This observation is consistent with previous reports suggesting that dimerization of LytA is independent of binding to choline (Usobiaga *et al.*, 1996). In addition, it suggested that the decreased autolytic activity of the LytA mutants is not owing to altered dimerization but is owing to impaired choline binding. Notably, the secondary-structure composition of LytA is nearly identical in the presence or absence of choline molecules (Supplementary Fig. S8*b*). Therefore, it suggested that choline binding would not be required for the folding of individual CBRs into the hairpin conformation. Altogether, our data indicated that all of the CBSs, which help LytA to anchor to the choline-containing TA chains, are required for LytA autolytic activity *in vivo*.

In agreement with previously reported structures of LytA-CBD, our structure shows that dimerization of full-length LytA is mediated by the C-terminal tail and CBR6 (Fig. 1*b*). As expected, deletion of the C-terminal tail resulted in a monomeric form of the truncated LytA fragment (residues Met1–Lys304; $LytA^{1-304}$) with almost no enzymatic activity towards either *S. pneumoniae* cells or purified TA-containing cell wall (Fig. 5). These data strongly support the longstanding hypothesis that dimerization is necessary for the autolytic activity of LytA (Sánchez-Puelles *et al.*, 1987). We conclude that both dimerization and choline binding are necessary, but either one is not sufficient, for the *in vivo* autolytic activity of LytA.

4. Discussion

Similar to previous structures of the incomplete CBD (Fernández-Tornero *et al.*, 2001, 2002), our full-length LytA also exhibits a boomerang-like dimer with the same dimeric interface. However, the crystal structure of the intact LytA

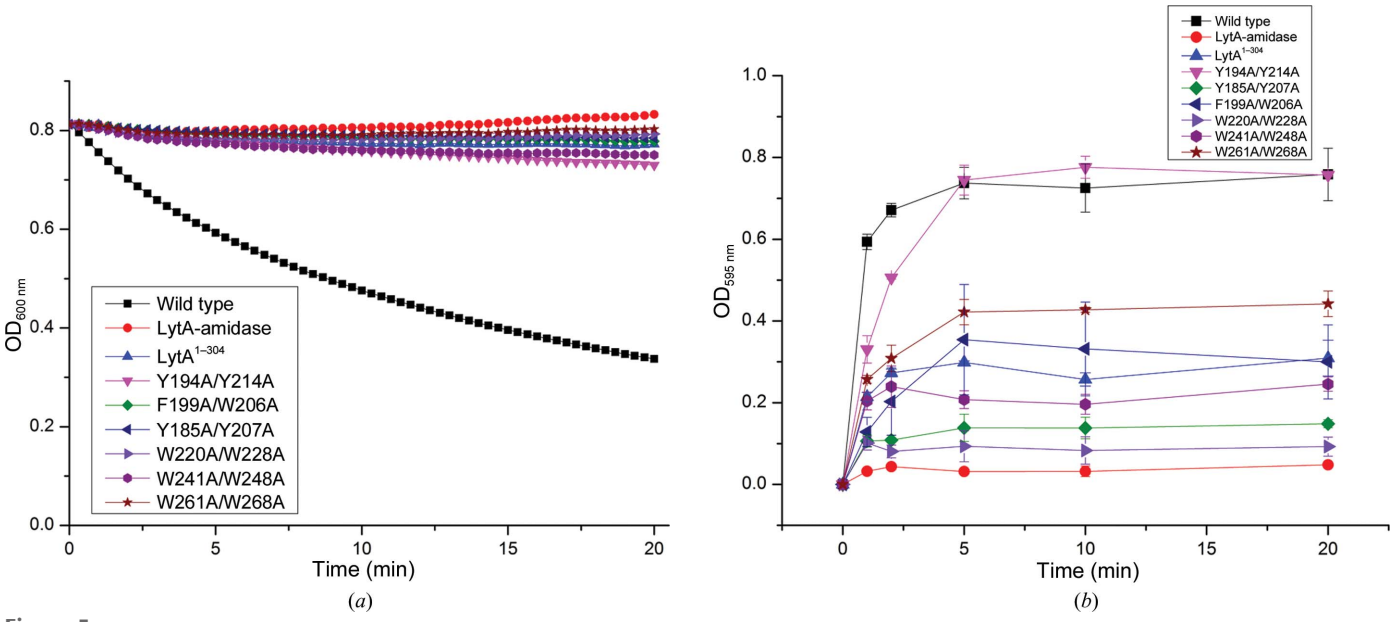

Figure 5
Enzymatic activity assays of LytA mutants. (*a*) Turbidometric assays. *S. pneumoniae* cells were treated with 10 µg ml^{-1} wild-type LytA, LytA-amidase, LytA$^{1–304}$ and CBS mutants, and the absorbance at 600 nm was recorded for 20 min at 20 s intervals. (*b*) Hydrolytic activity assays towards purified cell wall. Reactions containing RBB-labelled cell wall and 2 µ*M* wild-type LytA or LytA variants were incubated at 37°C for the indicated times. Undigested PG was pelleted by centrifugation and the absorbance of the supernatants at 595 nm was determined.

enabled us to clearly define the existence of six CBSs, five canonical CBSs and one single-layered CBS, in each subunit for the first time. Here, we found that double mutations at either type of CBS lead to a loss of autolytic activity towards *S. pneumoniae* under physiological conditions, which might be the consequence of impaired hydrolytic activity of the related mutants towards cell wall (Fig. 5), indicating that full occupancy of all CBSs is necessary for full activity of LytA. Meanwhile, the truncated LytA$^{1–304}$, which adopts a monomeric structure, showed no autolytic activity towards *S. pneumoniae* cells (Fig. 5). Altogether, these data therefore suggest that dimerization and full occupancy of all CBSs through binding to choline-containing TA chains of the cell wall enables LytA to adopt a boomerang-like dimeric conformation and acquire full activity.

It has been proposed that dimerization would allow LytA to cleave lactyl-amide bonds by a step-by-step mechanism without release from the cell wall (Fernández-Tornero *et al.*, 2002). However, the molecular details of such a mechanism remain unknown. To correlate the boomerang-like structure of LytA with its function *in vivo*, we docked the structure of full-length LytA into the *E. coli* PG network, which is the only PG network model available to date (Meroueh *et al.*, 2006). The pertinence of this model is however supported by the similar overall structure of Gram-positive and Gram-negative PG networks, despite differences in the PG thickness and the composition of the peptide stems (Silhavy *et al.*, 2010). Moreover, previous reports indicated that *E. coli* PG can be cleaved by LytA (Weidel & Pelzer, 1964). We therefore measured the distance between two lactyl-amide N atoms in the *E. coli* PG network model, and surprisingly found a mean distance of 103–105 Å (Fig. 6), which matches the distance between two active sites in the boomerang-like LytA dimer (Fig. 1*b*). We therefore propose a model in which the LytA dimer would sequentially cleave lactyl-amide bonds ∼103 Å apart. In this model, repetitive cycles of binding and release events between the choline-containing TA chains allow the

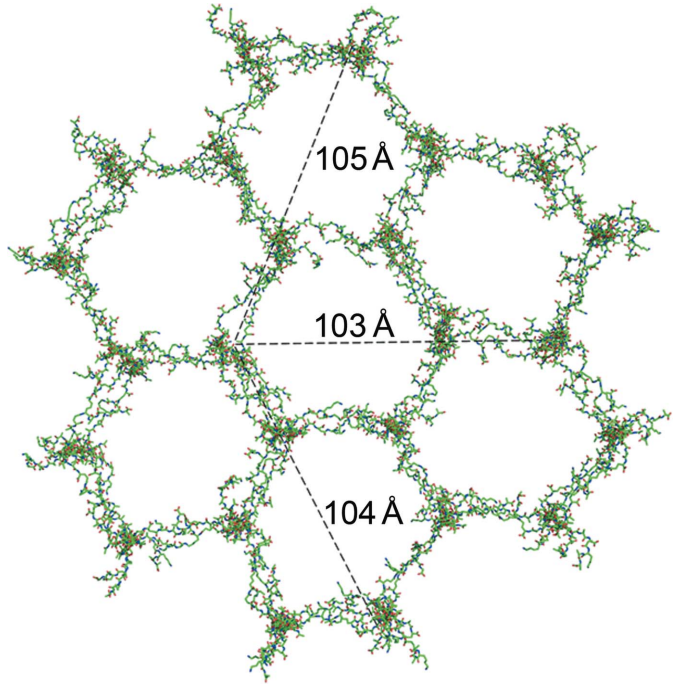

Figure 6
A model for cleavage of the PG network. A top view of the beehive-like *E. coli* PG network. The distances between two lactyl-amide bonds from a glycan chain and a third neighbouring chain are shown in Å.

amidase to walk step by step on the PG and cleave the polymer in a processive and efficient manner.

Acknowledgements

We greatly appreciate Professor Jing-Ren Zhang at Tsinghua University for providing the *lytA* mutant strain. We thank Professor Shahriar Mobashery at the University of Notre Dame for supplying the coordinates of *E. coli* peptidoglycan. We also thank the staff at Shanghai Synchrotron Radiation Facility for assistance in data collection. This work was supported by the Ministry of Science and Technology of China (Grant Nos. 2013CB835300 and 2014CB910100), the National Natural Science Foundation of China (Grant Nos. 31470739 and U1332114), the Fundamental Research Funds for the Central Universities and the Program for Changjiang Scholars and Innovative Research Team in University.

References

Adams, P. D. *et al.* (2010). *Acta Cryst.* D**66**, 213–221.
Brodersen, D. E., de La Fortelle, E., Vonrhein, C., Bricogne, G., Nyborg, J. & Kjeldgaard, M. (2000). *Acta Cryst.* D**56**, 431–441.
Büttner, F. M., Zoll, S., Nega, M., Götz, F. & Stehle, T. (2014). *J. Biol. Chem.* **289**, 11083–11094.
Chen, V. B., Arendall, W. B., Headd, J. J., Keedy, D. A., Immormino, R. M., Kapral, G. J., Murray, L. W., Richardson, J. S. & Richardson, D. C. (2010). *Acta Cryst.* D**66**, 12–21.
Cockeran, R., Anderson, R. & Feldman, C. (2002). *Curr. Opin. Infect. Dis.* **15**, 235–239.
DeLano, W. L. (2002). *PyMOL*. http://www.pymol.org.
Díaz, E., Munthali, M., Lünsdorf, H., Höltje, J. V. & Timmis, K. N. (1996). *Mol. Microbiol.* **19**, 667–681.
Emsley, P. & Cowtan, K. (2004). *Acta Cryst.* D**60**, 2126–2132.
Fernández-Tornero, C., García, E., López, R., Giménez-Gallego, G. & Romero, A. (2002). *J. Mol. Biol.* **321**, 163–173.
Fernández-Tornero, C., López, R., García, E., Giménez-Gallego, G. & Romero, A. (2001). *Nature Struct. Biol.* **8**, 1020–1024.
Garcia-Bustos, J. F. & Tomasz, A. (1987). *J. Bacteriol.* **169**, 447–453.
Gosink, K. K., Mann, E. R., Guglielmo, C., Tuomanen, E. I. & Masure, H. R. (2000). *Infect. Immun.* **68**, 5690–5695.
Hermoso, J. A., Lagartera, L., González, A., Stelter, M., García, P., Martínez-Ripoll, M., García, J. L. & Menéndez, M. (2005). *Nature Struct. Mol. Biol.* **12**, 533–538.
Holm, L. & Rosenström, P. (2010). *Nucleic Acids Res.* **38**, W545–W549.
Höltje, J. V. & Tomasz, A. (1976). *J. Biol. Chem.* **251**, 4199–4207.
Laskowski, R. A., MacArthur, M. W., Moss, D. S. & Thornton, J. M. (1993). *J. Appl. Cryst.* **26**, 283–291.
Mellroth, P., Daniels, R., Eberhardt, A., Rönnlund, D., Blom, H., Widengren, J., Normark, S. & Henriques-Normark, B. (2012). *J. Biol. Chem.* **287**, 11018–11029.
Mellroth, P., Sandalova, T., Kikhney, A., Vilaplana, F., Hesek, D., Lee, M., Mobashery, S., Normark, S., Svergun, D., Henriques-Normark, B. & Achour, A. (2014). *mBio*, **5**, e01120-13.
Meroueh, S. O., Bencze, K. Z., Hesek, D., Lee, M., Fisher, J. F., Stemmler, T. L. & Mobashery, S. (2006). *Proc. Natl Acad. Sci. USA*, **103**, 4404–4409.
Molina, R., González, A., Stelter, M., Pérez-Dorado, I., Kahn, R., Morales, M., Moscoso, M., Campuzano, S., Campillo, N. E., Mobashery, S., García, J. L., García, P. & Hermoso, J. A. (2009). *EMBO Rep.* **10**, 246–251.
Morlot, C., Uehara, T., Marquis, K. A., Bernhardt, T. G. & Rudner, D. Z. (2010). *Genes Dev.* **24**, 411–422.
Morris, G. M., Huey, R., Lindstrom, W., Sanner, M. F., Belew, R. K., Goodsell, D. S. & Olson, A. J. (2009). *J. Biol. Chem.* **30**, 2785–2791.
Mosser, J. L. & Tomasz, A. (1970). *J. Biol. Chem.* **245**, 287–298.
Murshudov, G. N., Skubák, P., Lebedev, A. A., Pannu, N. S., Steiner, R. A., Nicholls, R. A., Winn, M. D., Long, F. & Vagin, A. A. (2011). *Acta Cryst.* D**67**, 355–367.
Otwinowski, Z. & Minor, W. (1997). *Method Enzymol.* **276**, 307–326.
Sánchez-Puelles, J. M., García, J. L., López, R. & García, E. (1987). *Gene*, **61**, 13–19.
Seo, H. S., Michalek, S. M. & Nahm, M. H. (2008). *Infect. Immun.* **76**, 206–213.
Severin, A., Horne, D. & Tomasz, A. (1997). *Microb. Drug. Resistance*, **3**, 391–400.
Silhavy, T. J., Kahne, D. & Walker, S. (2010). *Cold Spring Harb. Perspect. Biol.* **2**, a000414.
Tomasz, A. (1967). *Science*, **157**, 694–697.
Tomasz, A. & Westphal, M. (1971). *Proc. Natl Acad. Sci. USA*, **68**, 2627–2630.
Tuomanen, E., Liu, H., Hengstler, B., Zak, O. & Tomasz, A. (1985). *J. Infect. Dis.* **151**, 859–868.
Usobiaga, P., Medrano, F. J., Gasset, M., Garciá, J. L., Saiz, J. L., Rivas, G., Laynez, J. & Menéndez, M. (1996). *J. Biol. Chem.* **271**, 6832–6838.
Varea, J., Saiz, J. L., López-Zumel, C., Monterroso, B., Medrano, F. J., Arrondo, J. L., Iloro, I., Laynez, J., Garcia, J. L. & Menéndez, M. (2000). *J. Biol. Chem.* **275**, 26842–26855.
Vollmer, W., Joris, B., Charlier, P. & Foster, S. (2008). *FEMS Microbiol. Rev.* **32**, 259–286.
Weidel, W. & Pelzer, H. (1964). *Adv. Enzymol. Relat. Areas Mol. Biol.* **26**, 193–232.
Winn, M. D. *et al.* (2011). *Acta Cryst.* D**67**, 235–242.
Zhou, R., Chen, S. & Recsei, P. (1988). *Anal. Biochem.* **171**, 141–144.
Zoll, S., Pätzold, B., Schlag, M., Götz, F., Kalbacher, H. & Stehle, T. (2010). *PLoS Pathog.* **6**, e1000807.